Seismic demand evaluation of reinforced-concrete buckling-restrained braces for precast concrete frames

Shane Oh, Jon Mohle, Lily A. Pearson, Mark P. Manning, Brad D. Weldon, and Yahya C. Kurama

- This study numerically investigated the expected dynamic seismic response demands of multistory precast concrete frame structures using a novel reinforced-concrete buckling-restrained brace component.
- A set of 26 braced frame archetypes were subjected to a set of 44 scaled ground motion records to quantify the maximum interstory drift, design story drift, brace ductility, cumulative brace ductility, and end gap closure.
- It was found that braces designed for a maximum design story drift of 4% and demonstrating ductility capacities of at least 51 and cumulative ductility capacities of at least 297 are needed for precast concrete braced frame structures in high seismic regions to satisfy the median collapse performance criteria in the Federal Emergency Management Agency's FEMA P695.

Several studies have investigated buckling-restrained braced frame structures for seismic regions.[1–8] These studies have primarily focused on frames with steel buckling-restrained braces. More recently, Oh et al.[9,10] proposed a novel reinforced-concrete buckling-restrained brace for use in an all–precast concrete lateral-load-resisting braced frame. Preliminary numerical[9] and experimental[10] investigations on this concrete brace have shown that critical failure modes must be addressed for the desired ductile behavior of the brace to be achieved. Continued experimental work toward this goal will require an assessment of the expected seismic demands for which the braces need to be designed and validated through testing. This paper quantifies these brace performance demands by numerically evaluating the nonlinear dynamic response of a set of 26 all–precast concrete braced frame archetypes.

Previous research

A recent numerical study[8] evaluated the seismic design of precast concrete building frames with traditional steel buckling-restrained braces using the procedures established by the Federal Emergency Management Agency's *Quantification of Building Seismic Performance Factors* (FEMA P695).[11] The numerical results of this study supported a response modification coefficient (R factor) of 8, the same value used in ASCE/SEI 7-22 for steel buckling-restrained braced frames.[12]

Kessler et al.[13] investigated the welded gusset plate connection between a steel buckling-restrained brace (simulated us-

ing a hydraulic actuator) and the beam and column members of a precast concrete building frame. This research revealed practical challenges to incorporating steel braces in precast concrete construction, mainly caused by possible misalignments and tolerance differences between the steel brace and the precast concrete frame.

Oh et al.[9] introduced and numerically investigated the isolated behavior of a novel reinforced-concrete buckling-restrained brace. This recent study is closely related to the current paper, which focuses on the seismic demands on this brace when it is used within a multistory precast concrete frame structure subjected to dynamic loading. **Figure 1** shows the single brace subassembly model investigated by Oh et al.[9] and also depicts the primary components of the brace. ASTM A706[14] reinforcing bars are designed as ductile yielding energy-dissipation components of the brace under reversed-cyclic loading, where unbonded (plastic-wrapped) lengths of the bars at each end of the brace are axially separated from the surrounding concrete. Under tension and compression loading of the brace, the axial deformations of the energy-dissipation bars are intended to be evenly (that is, near uniformly) distributed over this unbonded length. The unbonded length is designed so that the bars undergo large postyield strains in tension, but the maximum strains are limited so that fracture of the steel does not occur during the expected deformations of the brace in tension.

As an important detail, a small gap (a few inches wide) is designed at each end of the brace to allow the energy dissipation bars to yield in compression (that is, for the bars to freely compress) without the brace concrete contacting the adjacent column or beam corbel zone. This feature is important in developing a nearly symmetric tension-compression behavior of the brace and also limiting damage to the brace ends and corbel concrete.

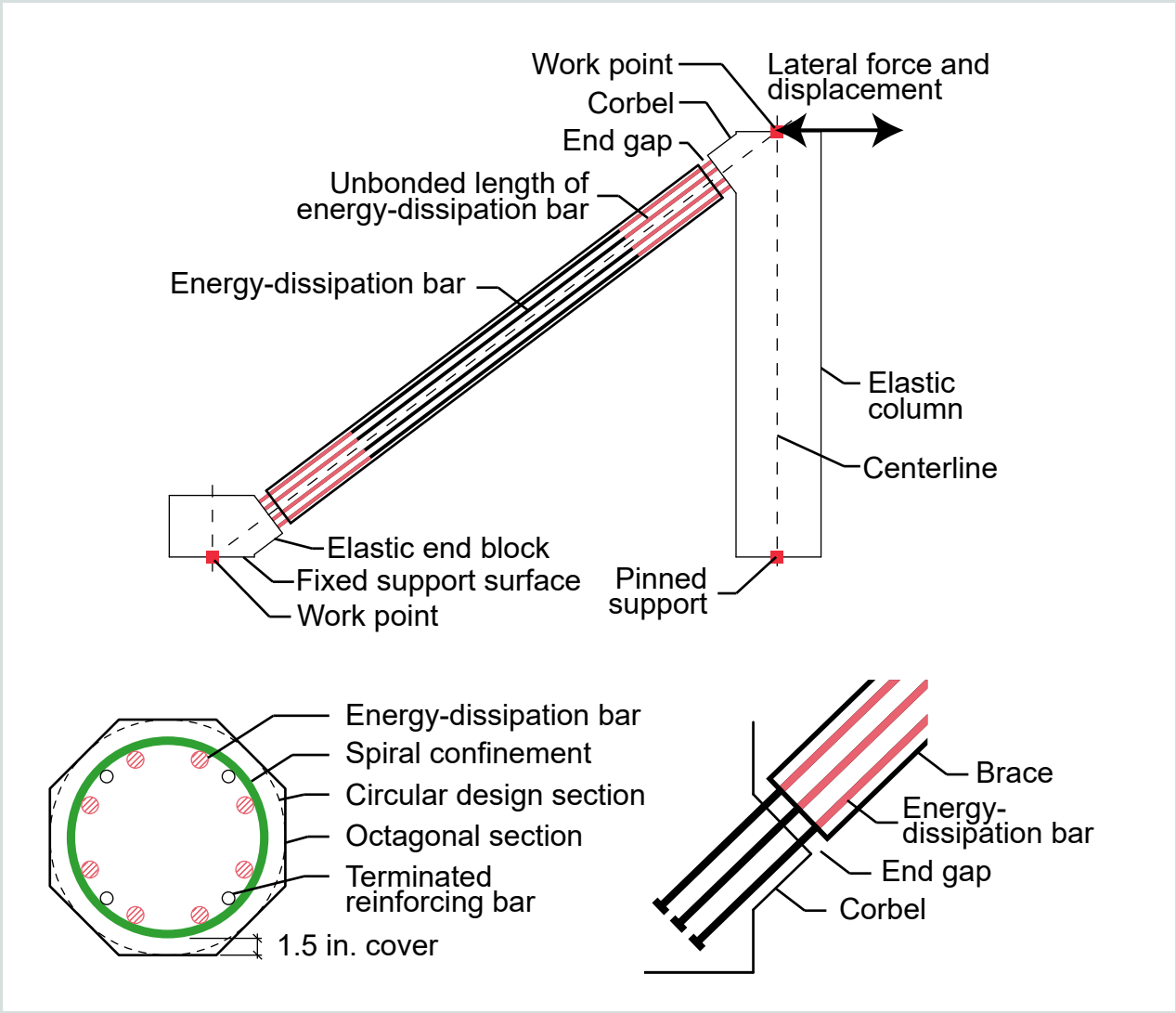

Figure 1. Isolated reinforced-concrete buckling-restrained brace subassembly, section view of brace, and brace-to-frame connection at end gap. Note: 1 in. = 25.4 mm.

Additional longitudinal reinforcing bars are bonded along the entire length of the brace to prevent the energy dissipation bars from yielding in the bonded (midlength) region of the brace. This reinforcement does not cross the end gaps of the brace (referred to as terminated reinforcement in the remainder of this paper). Thus, the axial stiffness, strength, and ductility of the brace are governed primarily by the deformations of the energy-dissipation bars within the unbonded regions and the end gaps.

Preliminary experiments of this novel brace were recently conducted by Oh et al.[10] in an isolated diagonal brace test setup similar to the arrangement shown in Fig. 1. The full intended ductile behavior of the brace could not be reached in these tests due to premature local buckling of the energy-dissipation bars over their unsupported lengths in the end gap regions. Thus, the design of these gaps is critical to the performance of the brace. The gaps must be sufficiently wide to prevent contact at the brace ends over the expected deformations of the brace in compression but not too wide so that local buckling of the energy-dissipation bars within this region can be prevented. The expected seismic demands to guide this and other design aspects of the brace are quantified in the current paper.

Research goals, contributions, and scope

To advance the exploration of all–precast concrete buckling-restrained braced frames, this study seeks to numerically investigate the dynamic demands on multistory frame structures utilizing the proposed brace subjected to earthquake loading. These quantified demands are intended to guide the design and testing of brace and frame specimens in future experimental research. To this end, 26 precast concrete braced frame archetypes were designed with features similar to those of the precast concrete archetypes with traditional steel buckling-restrained braces in Oh et al.[8] These frame designs using the novel braces were compared with the previous archetype designs using steel braces[8] in terms of brace yielding areas and frame lateral stiffnesses. Then, incremental dynamic time-history analyses were conducted to quantify the maximum brace ductility, cumulative brace ductility, interstory drift, design story drift, and gap closure demands for the novel brace. In these analyses, all braces were assumed to be adequately designed to prevent undesirable failure mechanisms (for example, buckling of the energy-dissipation bars), such that the analysis results establish the minimum capacities that the braces need to be designed and validated for in future experimental research.

Overview of archetype braced frames

The 26 all–precast concrete braced frame structure archetypes investigated in this paper were designed for the most critical building configurations and performance groups investigated by Oh et al.[8] for precast concrete frames with steel buckling-restrained braces. These archetypes span the expected design space of the proposed structural system, with different building plans, numbers of braced frames, brace configurations, and numbers of stories.

The archetypes were based on office and industrial building configurations with approximately 30,000 ft^2 (2800 m^2) floor areas and 15 to 25 ft (4.6 to 7.6 m) story heights.[8] The first office layout placed the braced frames toward the building core to intentionally introduce accidental torsion effects per ASCE/SEI 7-16.[15] The addition of torsional effects in these archetypes increased the lateral force demands compared with the same structure without torsional effects. All other building configurations placed the braced frames toward the outside of the building such that no accidental torsion effects were included in the design of these structures. Three different brace elevation configurations were investigated:

- single diagonal
- alternating single diagonal (also known as zigzag)
- chevron

The archetypes were then separated into seven different performance groups for system evaluation. The remainder of this paper labels each archetype using the same four-character identifiers in Oh et al.,[8] where the first character is the building plan number, the next two characters indicate the brace configuration (SD for single diagonal, ZZ for zigzag, and CC for chevron), and the last character is the number of stories. For example, archetype 1SD3 is a three-story frame with single-diagonal braces in building plan layout 1.

The precast concrete beam and column members of each archetype frame were designed using deformed steel reinforcement with no prestressing, considering details that emulate monolithic cast-in-place reinforced-concrete structures. Jointed (or nonemulative) precast concrete buckling-restrained braced frame structures[16] were not included in this study, but these types of precast concrete systems may be investigated in the future.

As discussed in Oh et al.,[8] large design axial tension forces in the beams and columns necessitated the use of higher-grade steel bars to minimize the member sizes while satisfying maximum reinforcements ratios. As such, the specified design yield strength of the reinforcing bars f_{sy} used within the beams and columns was 80 ksi (550 MPa). The specified design compressive strength of the concrete f'_c was 6 ksi (40 MPa).

The use of higher grade energy-dissipation bars is not desirable because this would reduce the brace axial stiffness by reducing the required bar areas to achieve the brace design axial strength. As such, the energy-dissipation bars in the buckling-restrained braces were designed with a minimum yield strength $f_{y,min}$ of 60 ksi (410 MPa) and maximum yield strength $f_{y,max}$ of 78 ksi (540 MPa), corresponding to the requirements of ASTM A706[14] for Grade 60 (410 MPa) reinforcing steel.

Design of archetype braced frames

To target similar lateral load behaviors, the seismic performance factors used in the design of the archetypes in this paper matched the values used for the archetypes with steel buckling-restrained braces in Oh et al.,[8] which include an R factor of 8, deflection amplification factor C_d of 8, and system overstrength factor Ω_0 of 2.5. Through this approach, the numerical results of the current study are intended to establish the minimum brace capacities (for example, brace ductilities) necessary for the future experimental evaluation and validation of these seismic performance factors for all–precast concrete buckling-restrained braced frames.

Design forces

The equivalent lateral force procedure from ASCE/SEI 7-16 with design spectral accelerations corresponding to seismic design category D_{max} (as in Oh et al.[8]) was used to represent the design of structures in high seismic areas. All archetypes were designed for previously defined gravity loads,[8] with the total average roof and floor dead loads taken as 160 lb/ft^2 (7660 N/m^2), including a precast concrete double-tee beam flooring system with a 4 in. (100 mm) thick cast-in-place concrete topping. The roof and floor average live loads were taken as 20 and 100 lb/ft^2 (960 and 4800 N/m^2), respectively.

Design of braces

For each archetype frame, once the ASCE/SEI 7-16 equivalent lateral forces were calculated, the factored brace design axial forces N_u were determined. Because the same archetype layouts and loads were used, the factored concrete brace design forces for the archetypes in this paper were identical to those for the steel braces in previous research.[8] The size and number of the energy-dissipation bars in the concrete braces were then chosen to meet the required yielding areas based on the assumed minimum yield strength, $f_{y,min}$ of 60 ksi (410 MPa), with the following considerations:

- Larger bar sizes were preferred because they are less susceptible to buckling and generally reduce congestion in the brace cross section.
- Per ACI 318-19[17] section 25.4.4.1, the maximum size of the energy-dissipation bars was limited to no. 11 (36M) for bars with headed end anchorages.
- At least four energy-dissipation bars were used to provide stability of the bar group across the end gaps where they are not laterally supported.
- An even number of energy-dissipation bars was used (this selection generally resulted in better placement of the bars through the reinforcement in the corbel, beam, and column regions).

The total area of the terminated longitudinal reinforcement A_{sT} was designed to be approximately 30% to 40% of the total provided energy-dissipation bar area A_{ED}. Then, the gross cross-sectional area of each brace was determined to result in a total longitudinal steel reinforcement ratio (including all the energy-dissipation and additional terminated bars) of approximately 6%.

The required unbonded length of the energy-dissipation bars at the ends of each brace was determined to ensure that the maximum tensile strain of the bars does not reach the design usable tensile strain limit $\varepsilon_{s,max}$ at a maximum design story drift $\Delta_{d,max}$ of 3%. Based on cyclic uniaxial testing of energy-dissipation bars in Aragon et al.,[18] the usable tensile strain limit $\varepsilon_{s,max}$ for the bars was taken as 0.06. Further information on the design of the unbonded lengths, which used a simplified shear frame model to determine the brace elongation from the maximum design story drift, can be found in Oh et al.[9] The validity of this simplified shear frame model is evaluated later in this paper.

Design of beams and columns

The beam and column components of each archetype frame were designed based on the applied gravity loads and the adjusted brace forces following the capacity-based approach outlined in Oh et al.[8] with ASCE/SEI 7-16 load combinations 2, 6, and 7. The adjusted brace forces were calculated using a maximum yield strength $f_{y,max}$ of 78 ksi (540 MPa) and an assumed strain-hardening factor ω of 1.3 for the energy-dissipation bars to represent the maximum axial forces in the braces during an earthquake.

The beams and columns were designed as rectangular sections with ASTM A706[14] Grade 80 (550 MPa) longitudinal reinforcement ratios between 1% and 6% (ACI 318-19 section 18.7.4.1). All beams were designed with a 4 in. (100 mm) thick cast-in-place concrete topping slab assumed to act compositely with the beam. Based on the proposed casting of the novel brace within an entire frame story unit as described in Oh et al.,[9] the beams and columns in each story unit were designed to have the same width to ease forming and casting at the precast concrete production facility. However, in cases where the frame design was controlled by the allowable drift requirements of ASCE/SEI 7-16, the beam and column widths were optimized to minimize frame overstrength, thus resulting in more critical structures for the dynamic response analyses.

Effective linear-elastic braced frame analyses for allowable drift design

Each archetype frame was modeled linear elastically with effective (reduced) stiffness factors for the beam, column, and brace components to provide a representation of the maximum story drifts at the design equivalent lateral force level. All models had fixed column bases and fixed beam-to-column connections. The beams and columns were modeled using the same axial and flexural effective stiffness reduction factors as those in Oh et al.[8]

Each brace was modeled using a single linear-elastic truss element extending from work point–to–work point (at the intersections between the brace and column/beam centerlines [Fig. 1]). The cross-sectional area of this truss element was taken as the total energy-dissipation bar area A_{ED}, with modulus of elasticity of steel E_s, and a stiffness modification factor KF was applied considering the axial stiffnesses of the unbonded and bonded regions of the brace in series as calculated in Eq. (1).

$$KF = \frac{L_T}{L_{ub}}\left(\frac{k_b}{k_{ub}+k_b}\right) \quad (1)$$

where

L_T = work point–to–work point diagonal length of brace

L_{ub} = total length of unbonded regions at both ends of brace

k_b = effective axial stiffness of bonded region = E_bA_b/L_b

E_b = effective modulus of elasticity of bonded region

A_b = effective area of bonded region

L_b = length of bonded region

k_{ub} = effective axial stiffness of unbonded regions = E_sA_{ED}/L_{ub}

The effective stiffness for the unbonded regions k_{ub} was calculated based solely on the energy-dissipation bars. For the bonded region, different effective stiffnesses were used in tension and in compression. In tension, the bonded region will crack. Thus, the effective area A_b was calculated as the total area of the longitudinal reinforcing steel A_s, which includes the area of the energy-dissipation bars A_{ED} and the area of the additional terminated reinforcing bars A_{sT}, and the modulus of elasticity E_b was taken as the steel modulus of elasticity E_s. In compression, the bonded region was assumed to be uncracked. Thus, A_b was calculated as the uncracked transformed area A_{ut} of the reinforced-concrete section and E_b was taken as the concrete modulus of elasticity E_c. Based on these assumptions, the calculated KF values for the braces in the archetype frames ranged from 1.20 to 1.36 in tension and 2.24 to 2.46 in compression.

The effective brace stiffnesses calculated using Eq. (1) were verified using the continuum nonlinear finite element model[19] described in Oh et al.[9,10] **Figure 2** shows one of these stiffness comparisons, where strain was calculated as the total axial deformation between the work points of the brace divided by the work point–to–work point length L_T and stress was calculated as the total brace axial force divided by the energy-dissipation steel area A_{ED}. The calculated stiffnesses were reasonably close to (within 5% of) the stiffnesses from the finite element models. Experimental validation of the finite element model stiffnesses for the reinforced-concrete brace can be found in Oh et al.[10]

The end zones of each brace from the face of the corbel to the work point location at each end were not designed in this research. Instead, these regions were assumed to have the same effective stiffnesses as the middle-bonded region of the brace in both tension and compression. Subsequently, the lengths of these end zones were added to the length of the bonded region. Modeling the end zones in this way resulted

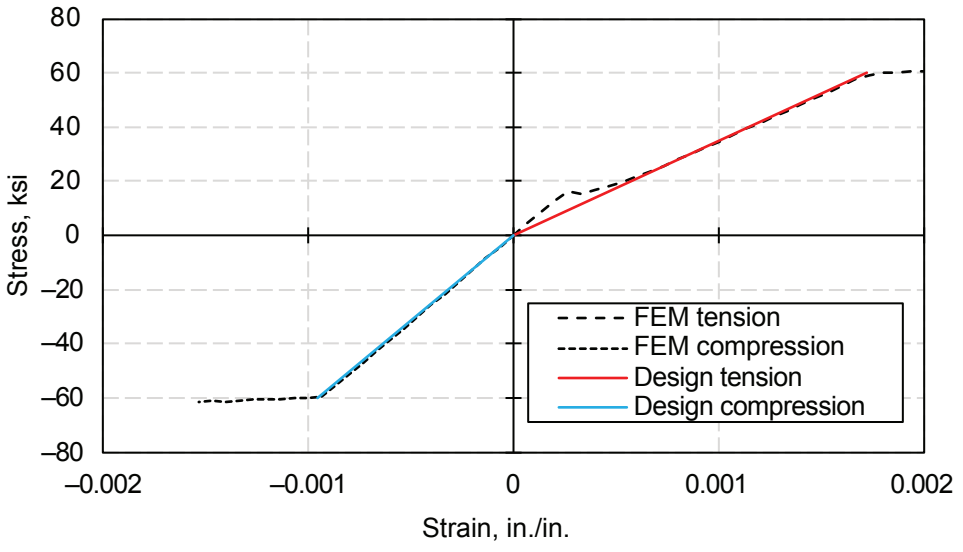

Figure 2. Comparison of effective stiffnesses from design equations and continuum finite element model (FEM) results. Note: 1 in. = 25.4 mm; 1 ksi = 6.895 MPa.

in a lower effective stiffness and was deemed conservative for the allowable drift checks. This is because the end zones of a brace have larger cross sections and more reinforcement than the brace and may crack less than the middle-bonded region.

Debonding of the energy-dissipation bars due to penetration of yielding into the bonded regions can occur under reversed-cyclic loading. The unbonded lengths of each brace were increased to account for this effect because it results in a reduced effective stiffness for the brace. The total additional unbonded length $L_{ub,add}$ was calculated using Eq. (2).

$$L_{ub,add} = 4\alpha_b d_b \quad (2)$$

where

α_b = coefficient quantifying effective additional debonded length

d_b = energy-dissipation bar diameter

The factor 4 in Eq. (2) accounts for the four transition zones between the unbonded and bonded regions for the energy-dissipation bars along the length of the brace. ACI 550.7[20] gives a range of 2.0 to 5.5 for the coefficient quantifying effective additional debonded length α_b. Other research[21] has shown α_b to be approximately 2.0 for energy-dissipation bars stressed well into the nonlinear range. These α_b values were determined based on experimental tests where the reinforcing bars were stressed under flexural cyclic loads. In contrast, the energy-dissipation bars in the proposed brace are stressed under axial full-reversed cyclic load, which may result in greater debonding than that observed in previous flexural tests. Given the lack of more representative experimental data, the mid-range value of the coefficient quantifying effective additional debonded length α_b of 3.75 from ACI 550.7[20] was used in the modeling of the braces in this research. Future experimental work should investigate the additional debonded lengths under the loading conditions that the brace energy-dissipation bars are expected to experience.

As shown in Fig. 2 and experimentally demonstrated in Oh et al.,[10] cracking of the bonded regions resulted in a significantly smaller stiffness of the reinforced-concrete braces in tension than in compression. Therefore, asymmetric braced frame layouts (those with single-diagonal and zigzag brace configurations in this research) had significantly larger story drifts when the direction of lateral loading coincided with all or more of the braces being subjected to tension forces. To prevent the smaller tension stiffness of the braces from dominating the drift control design of the archetypes with asymmetric brace layouts, the effective linear-elastic models of these structures considered two superimposed frames with braces oriented in opposite directions, assuming rigid floor and roof diaphragms for the buildings. **Figure 3** shows a representation of this modeling technique, which was possible because all the archetype building layouts had an even number of braced frames. The gravity loads were also doubled for these double-frame analyses.

As described in Oh et al.,[8] the allowable drift design for each archetype frame was conducted iteratively due to the dependence of the beam and column effective moment of inertia (flexural stiffness) reduction factors on the factored design axial force P_u and bending moment M_u. If the calculated story drifts exceeded the allowable limit per ASCE/SEI 7-16 Table 12.12-1 (2.5% drift for structures with four or fewer stories and 2% drift for all other structures), the energy-dissipation bar areas of the braces, cross-section dimensions of the braces (to maintain a total longitudinal steel reinforcement ratio of approximately 6%), and the cross-section dimensions of the columns over the entire frame height were scaled up until the drift requirements were met. Beam sizes were not changed

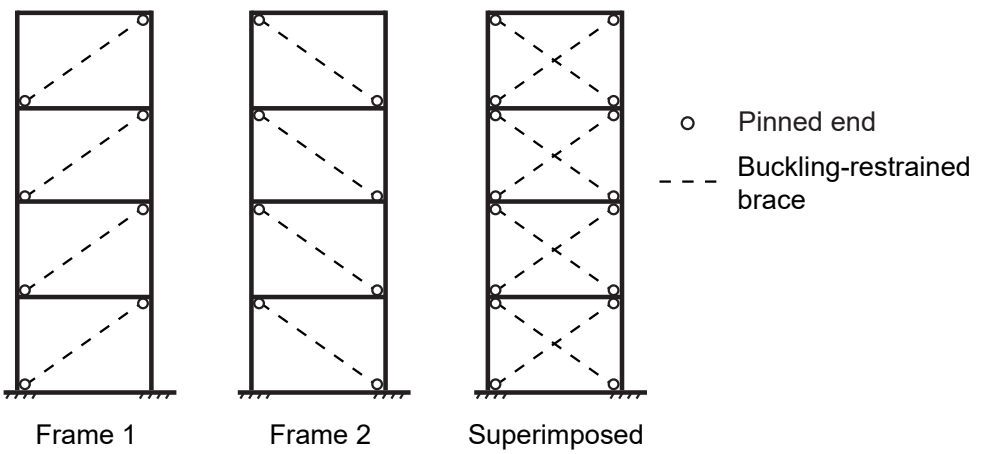

Figure 3. Superimposed asymmetric frames.

because the beam dimensions were found to have a relatively small effect on the maximum story drifts of the frames.

Comparison of archetype frame designs with reinforced-concrete and steel braces

Table 1 compares the brace yielding areas, yielding lengths, and maximum design story drifts for the archetype frames investigated in this paper with the same archetypes designed using conventional steel buckling-restrained braces in Oh et al.[8] (values shown in parentheses). Structures with drift-controlled designs were not included in the drift comparisons because the

Table 1. Comparison of archetype frame designs with reinforced-concrete and steel braces

Performance group	Archetype design identifier*	Range of brace yielding areas, in.^{2}	Range of brace yielding lengths, in.	Maximum drift, %	Ratio of maximum drifts
1	1SD1	3.2 (4.9)	89 (197)	1.43 (0.98)	1.47
	1SD2	4.7 to 6.2 (6.5 to 9.9)	89 to 95 (170 to 188)	1.69 (1.72)	0.98
	1SD3	4.0 to 7.6 (6.2 to 12.2)	91 to 93 (164 to 198)	2.13 (1.37)	1.55
2	2SD1	2.4 (3.8)	87 (186)	1.01 (1.21)	0.84
	2SD2	3.2 to 4.7 (5.1 to 7.6)	89 (186 to 192)	1.16 (1.45)	0.80
	2SD3	3.2 to 6.0 (4.8 to 9.4)	89 to 93 (182 to 193)	1.52 (1.59)	0.95
	4SD1	4.0 (6.1)	140 (382)	1.72 (1.35)	1.27
	4SD2	4.0 to 6.0 (6.3 to 9.2)	140 (336 to 395)	1.77 (1.45)	1.22
3	1SD6†	4.0 to 9.4 (4.7 to 14.7)	89 to 99 (158 to 190)	n/a	n/a
	1SD9†	4.7 to 15.6 (4.0 to 16.6)	89 to 99 (129 to 198)	n/a	n/a
	2SD6†	3.2 to 7.6 (3.6 to 11.3)	89 to 95 (176 to 201)	n/a	n/a
	2SD9†	2.4 to 7.6 (3.1 to 12.6)	87 to 93 (154 to 215)	n/a	n/a
4	2CC1	3.2 (2.9)	89 (202)	1.45 (1.46)	0.99
	2CC2	3.2 to 4.0 (3.8 to 5.9)	89 to 91 (191 to 199)	1.72 (1.49)	1.16
	2CC3	3.2 to 4.7 (3.6 to 7.1)	89 to 91 (186 to 199)	1.76 (1.45)	1.21
	5CC1	3.2 (3.3)	80 (311)	2.18 (1.40)	1.55
	5CC2	3.2 to 4.7 (3.5 to 5.0)	80 (302 to 310)	1.65 (1.54)	1.07
5	2CC4	3.2 to 4.7 (3.2 to 3.7)	89 to 91 (184 to 201)	0.90 (1.61)	0.56
	2CC6†	4.0 to 6.2 (2.7 to 8.5)	89 to 95 (178 to 202)	n/a	n/a
	2CC9†	4.7 to 7.9 (2.3 to 9.6)	89 to 95 (163 to 196)	n/a	n/a
6	2ZZ2	3.2 to 4.7 (5.1 to 7.6)	89 (186 to 192)	1.65 (1.52)	1.08
	2ZZ3	3.2 to 6.0 (4.8 to 9.4)	89 to 93 (182 to 193)	1.88 (1.60)	1.17
	4ZZ2	4.0 to 6.0 (6.3 to 9.2)	140 (336 to 395)	1.86 (1.52)	1.23
7	2ZZ4	3.2 to 6.2 (4.3 to 10.1)	89 to 95 (180 to 194)	2.01 (1.65)	1.21
	2ZZ6	4.0 to 7.9 (3.6 to 11.3)	89 to 95 (178 to 196)	1.89 (1.97)	0.96
	2ZZ9†	3.2 to 10.0 (3.1 to 12.5)	89 to 93 (155 to 215)	n/a	n/a

Source: Data for values in parentheses from Oh et al.[8]

Note: 1 in. = 25.4 mm; n/a = not applicable.

* The first character is the building plan number, the next two characters indicate the brace configuration (SD for single diagonal, ZZ for zigzag, and CC for chevron), and the last character is the number of stories.

† Drift-controlled design (maximum drift comparison not relevant).

designs of these structures were adjusted to satisfy the ASCE/SEI 7-16 allowable drift limit. Overall, the yielding steel areas were smaller and the yielding lengths (unbonded lengths plus end gap widths) were shorter for the reinforced-concrete braces compared with the steel braces in equivalent structures. The maximum design story drifts were on average about 20% greater than the archetypes using steel braces even after considering superimposed double frames to eliminate effects from asymmetric brace layouts and designing columns with more efficient rectangular cross sections, rather than square column sections for the archetypes in Oh et al.[8]

The greater maximum story drifts of the archetype frames using reinforced-concrete braces indicate smaller lateral stiffnesses of these frames compared with frames using conventional steel buckling-restrained braces. This is a potential disadvantage because it results in more drift-controlled designs for the new system, driven by two factors. First, the conventional braces in Oh et al.[8] were designed using steel yielding cores (plates) with a minimum yield strength of 38 ksi (260 MPa) while the proposed concrete braces were designed using Grade 60 (410 MPa) energy-dissipation reinforcing bars. The larger steel yield strength resulted in reduced yielding steel areas (and thus, reduced axial stiffnesses) for the concrete brace despite being designed for the same axial force as a conventional steel brace. Second, cracking of the bonded regions in the concrete braces led to much smaller stiffnesses in tension versus compression compared with the difference in the tension versus compression stiffnesses of a steel brace.

To investigate potential ways to increase the axial stiffness of the reinforced-concrete brace, **Fig. 4** shows the effects of the terminated reinforcement ratio and energy-dissipation steel yield strength (reinforcing bar grade) on the brace stiffnesses in tension and compression (for constant brace axial force) using Eq. (1). The amount of terminated reinforcement has a small effect on the brace stiffness, with the increase in steel ratio reaching unrealistic values before any significant increase in the tension stiffness of the brace is achieved. In contrast, the yield strength of the energy-dissipation bars has a substantially greater effect on the brace stiffnesses, with smaller yield strengths resulting in larger yielding steel areas and brace stiffnesses for a given brace axial force. Future research may consider investigating energy-dissipation bars with yield strengths smaller than 60 ksi (410 MPa); however, lack of availability of lower grade reinforcing bars, especially in larger diameters, is likely a key limiting factor for practical application in the United States.

Nonlinear numerical modeling

Nonlinear models of the archetypes were developed in the Open System for Earthquake Engineering Simulation (OpenSees) structural analysis platform. Archetypes with asymmetric (single-diagonal and zigzag) brace configurations were modeled as two superimposed frames with doubled gravity loads and seismic masses, similar to the linear-elastic drift analysis models. The seismic masses were assigned to the work point nodes of the frame. All models had fixed column bases with tributary dead D and live L gravity loads applied per the expected median gravity load combination $1.05D + 0.25L$. To account for second-order effects from gravity loads not tributary to the frame, a leaning column was pin-connected to the frame, similar to the nonlinear modeling of the archetypes with steel braces in Oh et al.[8] The beam and column components of the archetypes were modeled using axial-flexural fiber elements with longitudinal steel and concrete fibers. Details on the modeling of these components can be found in Oh et al.[8] and are not repeated herein. Though the archetypes analyzed in Oh et al.[8] use steel buckling-restrained braces, the validation of the numerical modeling of these structures based on shake table tests of multistory frames is a testament to the accuracy in the modeling of not just the braces but also the beams and columns. The same modeling parameters were adopted for the beams and columns of the archetypes with reinforced-concrete braces herein.

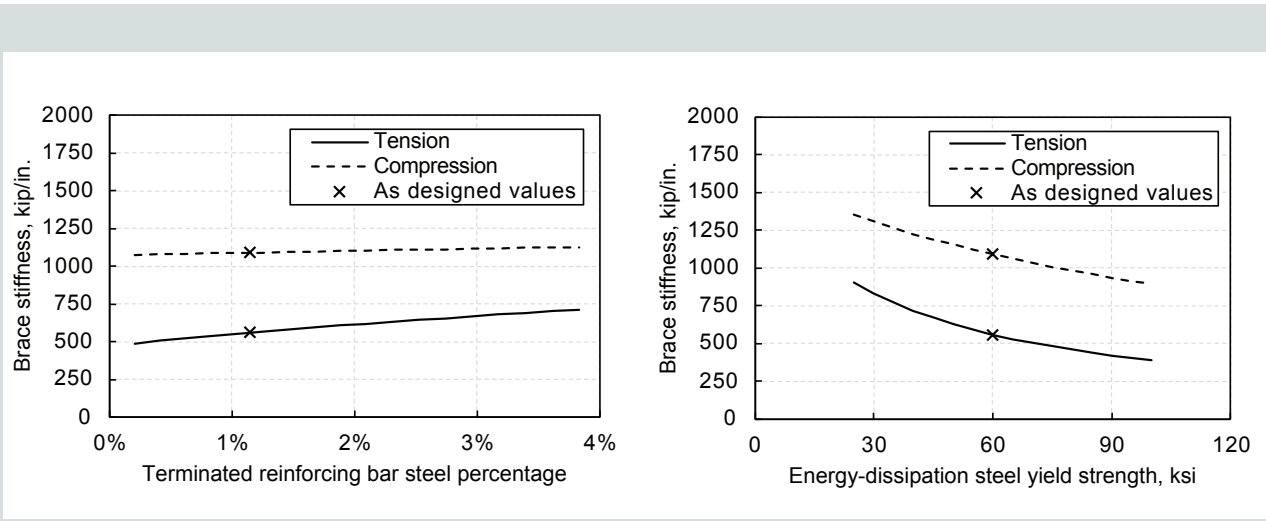

Figure 4. Effects of terminated steel reinforcement ratio and energy-dissipation steel yield strength on brace axial stiffness for constant brace axial force. Note: 1 in. = 25.4 mm; 1 kip = 4.448 kN; 1 ksi = 6.895 MPa.

Rather than separately modeling the bonded, unbonded, and end zone regions, each brace was modeled using a single truss element with area equal to the total area of the energy-dissipation bars A_{ED} and pinned at the work point locations (in other words, an element length equal to L_T), similar to the effective linear-elastic drift model described previously. However, unlike the effective linear-elastic brace element, the nonlinear brace element could not be modeled with a single stiffness modification factor *KF*. Instead, the Series material type in the structural analysis platform was used to combine the stiffnesses of the bonded and unbonded regions of the brace. In this material type, the stresses of the constituent materials are equal while the strains and flexibilities are added in series.

Each Series element modeling a brace comprised the Elastic and Steel4 material types in the structural analysis platform (**Fig. 5**). The Elastic material accounted for the stiffness of the middle-bonded region and the two end regions. Similar to the effective linear-elastic model described previously, these regions of the brace were assumed to be in the uncracked linear-elastic range of behavior in compression (with stiffness equal to the concrete modulus of elasticity E_c) and in the cracked linear-elastic range of behavior in tension (with stiffness equal to the steel modulus of elasticity E_s). The Steel4 material represented the unbonded regions of the brace, with the nonlinear cyclic stress-strain behavior for ASTM A706[14] Grade 60 (410 MPa) reinforcing bars, assuming that all of the nonlinear behavior of the brace concentrated in the unbonded regions. The length of the unbonded regions was increased by a total additional unbonded length $L_{ub,add}$ due to debonding of the energy-dissipation bars as given by Eq. (2).

The material stiffnesses of the bonded and unbonded regions (represented by the Elastic and Steel4 materials, respectively) were scaled using length and area ratios such that the combined Series truss element with area equal to A_{ED} and length equal to L_T provided a nonlinear axial force versus deformation behavior equivalent to the actual brace. **Table 2** shows the equations used to calculate the material stiffness multipliers for the bonded and unbonded regions of the brace. The stress-strain relationships shown in Fig. 5 for the bonded and unbonded regions were scaled using these multipliers. This simplified nonlinear structural analysis modeling approach for the braces was validated using the continuum nonlinear finite element model described in Oh et al.[9]

Analysis methodology for demand quantification

The design of the archetypes and selection of the ground motion records used in the dynamic analyses were important factors affecting the demand quantification. For example, structures with unrealistic overstrength or ground motions with

Table 2. Material stiffness multipliers for bonded and unbonded brace regions

Region	Compression	Tension
Bonded (Elastic)	$\left(\frac{A_{ut}}{A_{ED}}\right)\left(\frac{L_T}{L_b}\right)$	$\left(\frac{A_s}{A_{ED}}\right)\left(\frac{L_T}{L_b}\right)$
Unbonded (Steel4)	$\left(\frac{L_T}{L_{ub}}\right)$	

Note: A_{ED} = area of energy-dissipation bars; A_s = total longitudinal reinforcing steel area of brace, including energy-dissipation bars and terminated bars; A_{ut} = uncracked transformed area of reinforced concrete brace section; L_b = length of bonded regions, including middle region and end regions (from each corbel face to the work point location); L_T = total work point–to–work point diagonal length of brace; L_{ub} = total length of unbonded regions at both ends of brace, including an additional unbonded length $L_{ub,add}$ as given by Eq. (2).

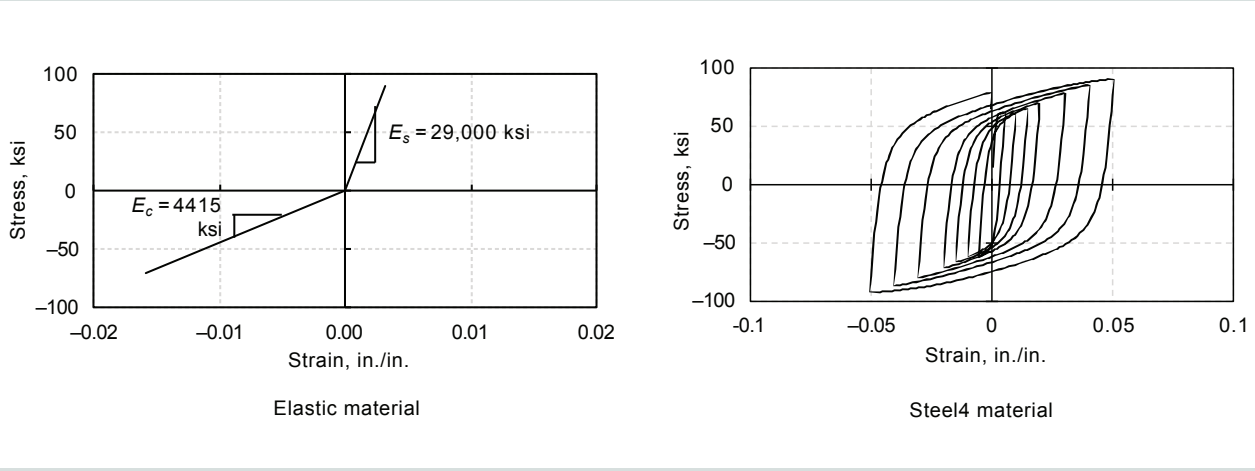

Figure 5. Materials used in Series element for nonlinear modeling of the braces—Elastic material for bonded regions and Steel4 material for unbonded regions—prior to application of stiffness multipliers. Note: 1 in. = 25.4 mm; 1 ksi = 6.895 MPa.

unrealistic intensity could result in unrealistic demands. As such, the demands were determined for structures designed and analyzed according to FEMA P695,[11] which provides a widely used methodology to formalize the determination of seismic performance factors (for example, the *R* factor) for new proposed lateral-force-resisting systems. The use of this methodology was intended to calculate expected demands in order to guide future experimental testing of the braces. Specifically, if future experimental research can demonstrate that the proposed brace can satisfy the demands quantified in this paper, then frame structures using these braces can be designed to satisfy the collapse performance requirements of FEMA P695.

The demand quantification analyses were conducted using the 44 ground motion records prescribed by FEMA P695. In this methodology, each ground motion was first normalized by its respective peak ground velocity. Then, each archetype was subjected to this normalized set of 44 records at increasing intensities (based on the median spectral acceleration of the entire set) until the collapse of the structure was deemed to occur under at least half of the 44 records. This intensity, referred to as the median collapse intensity S_{ct}, was then used to calculate an adjusted collapse margin ratio (ACMR)[11] for the archetype, where a higher ACMR indicates a lower probability of collapse.

Oh et al.[8] found that brace failure is the governing collapse criterion for precast concrete frames with conventional steel buckling-restrained braces. In the proposed structure with reinforced-concrete braces, this failure would be reached when the energy-dissipation bars reach their maximum ductility capacity or cumulative ductility capacity under the required condition that buckling of the bars across the end gaps is prevented. Rodriguez et al.[22] conducted tests of buckling-restrained reinforcing bars in Mexico (comparable to ASTM A706[14] Grade 60 [410 MPa] reinforcing bars) subjected to large tension-compression strains, similar to the intended use of the energy-dissipation bars in the proposed brace. The results showed that when buckling was prevented, the tested bars could reach total strain ranges of at least 0.15 (an applied maximum tension-compression strain range of 0.12 to -0.03), corresponding to a maximum ductility range of 72.5 and cumulative ductility of over 500. Based on these test results, a maximum ductility range of 58 (corresponding to an approximate total strain range of 0.12) and cumulative ductility of 350 were assumed for the energy-dissipation bars in all the archetypes in this study.

Table 3 shows the ACMR values and corresponding median collapse intensity S_{ct} values using the brace maximum ductility and cumulative ductility failure criteria above for each archetype. As described in Oh et al.,[8] these ACMR values were determined by identifying the lowest ground motion intensity (spectral acceleration) that caused failure of each archetype under half (22) of the record set. The archetype demands presented in the next section correspond to this median collapse intensity level for the 44 records.

This procedure resulted in a different median collapse intensity S_{ct} for each of the 26 archetypes when they were subjected to the FEMA P695 ground motion set. Nonlinear static pushover analyses of the archetypes were also conducted to determine the system overstrength per FEMA P695. The results of these analyses (Table 3) show that the precast concrete archetypes with concrete buckling-restrained braces had the same system overstrength factor Ω_0 of 2.5 as for precast concrete frames with steel braces as well as for steel buckling-restrained braced frames.[1] This is important for the dynamic demand evaluation because structures with higher overstrength would be expected to result in lower seismic deformation demands. The dynamic analysis results confirm that all the archetypes satisfied the minimum ACMR limits corresponding to acceptable collapse probabilities based on FEMA P695. As stated previously, this indicates that if future experimental research can demonstrate brace capacities that satisfy the performance targets—or demands—quantified in this paper, structures using these braces would likely satisfy the seismic collapse criteria in FEMA P695.

Per FEMA P695, the value of the *R* factor used in design is deemed acceptable when both of the following conditions are satisfied:

- The average ACMR for the archetypes in each performance group is greater than or equal to the 10% ACMR limit.
- The ACMR value for each archetype is greater than or equal to the 20% ACMR limit.

The 10% and 20% ACMR limits used for the archetype frames in Table 3 are the same as those used for precast concrete frames with conventional steel buckling-restrained braces investigated by Oh et al.[8] These same minimum ACMR limits were selected to allow for more direct comparisons between structures designed using the same *R* factor of 8 but with different types of braces (reinforced concrete versus steel). As described in Oh et al.,[8] the FEMA P695 minimum ACMR limits are based on a total system collapse uncertainty calculated from a prescribed record-to-record variability and a qualitative assessment of uncertainties in design requirements, test data, and modeling for the proposed system. In this study, all three uncertainties were rated as "good," resulting in minimum ACMR limits of 1.96 and 1.56 for 10% and 20% collapse probabilities, respectively. More information on these ACMR limits can be found in Oh et al.[8] The minimum ACMR limits would increase with greater uncertainty, resulting in larger quantified seismic demands for the system.

Demand quantification results

The dynamic analyses of the 26 archetypes under the 44 ground motion records (scaled collectively to the median collapse intensities S_{ct} listed in Table 3) resulted in a total of $26 \times 44 = 1144$ values for each demand considered, which included the maximum brace ductility μ_{max}, maximum cumulative brace

Table 3. Summary of nonlinear pushover and dynamic analysis results of archetype frames with reinforced-concrete braces

Performance group	Archetype design identifier*	Overstrength and collapse parameters			
		Ω_0	S_{ct}	ACMR	ACMR limit†
1	1SD1	2.31	1.30	2.07	1.56
	1SD2	1.99	1.68	2.45	1.56
	1SD3	1.90	1.72	2.36	1.56
	Group 1 mean	2.06	1.57	2.29	1.96
2	2SD1	2.55	1.30	2.05	1.56
	2SD2	1.95	1.47	2.14	1.56
	2SD3	1.86	1.51	2.07	1.56
	4SD1	2.21	1.51	2.37	1.56
	4SD2	1.72	1.60	2.15	1.56
	Group 2 mean	2.06	1.48	2.16	1.96
3	1SD6	2.31	1.85	2.45	1.56
	1SD9	3.33	1.47	1.81	1.56
	2SD6	2.00	1.68	2.28	1.56
	2SD9	2.50	1.22	1.57	1.56
	Group 3 mean	2.53	1.55	2.03	1.96
4	2CC1	2.76	1.30	2.11	1.56
	2CC2	1.84	1.51	2.20	1.56
	2CC3	1.72	1.47	2.01	1.56
	5CC1	2.25	1.26	2.05	1.56
	5CC2	1.58	1.51	2.20	1.56
	Group 4 mean	2.03	1.41	2.12	1.96
5	2CC4	1.56	1.55	2.13	1.56
	2CC6	1.75	1.68	2.42	1.56
	2CC9	2.23	2.23	3.08	1.56
	Group 5 mean	1.85	1.82	2.54	1.96
6	2ZZ2	1.95	1.47	2.14	1.56
	2ZZ3	1.88	1.51	2.07	1.56
	4ZZ2	1.72	1.60	2.15	1.56
	Group 6 mean	1.85	1.53	2.12	1.96
7	2ZZ4	1.73	1.55	2.08	1.56
	2ZZ6	2.17	1.85	2.62	1.56
	2ZZ9	2.76	1.51	1.98	1.56
	Group 7 mean	2.22	1.64	2.22	1.96

Note: ACMR = adjusted collapse margin ratio; S_{ct} = median collapse intensity; Ω_0 = system overstrength factor.

* The first character is the building plan number, the next two characters indicate the brace configuration (SD for single diagonal, ZZ for zigzag, and CC for chevron), and the last character is the number of stories.

† Per FEMA P695, the ACMR limit listed for the individual archetypes is for 20% collapse probability and the ACMR limit listed for the performance group mean is for 10% collapse probability.

ductility μ_c, maximum brace end gap closure $\Delta_{b,gap}$, maximum interstory drift Δ_{story}, and maximum design story drift $\Delta_{d,max}$. As an example, **Fig. 6** shows the maximum brace ductility μ_{max} demands for the 26 archetypes plotted against the spectral acceleration of the 44 records at the fundamental period of each archetype (after the ground motion set was collectively scaled to the median S_{ct} intensity for the archetype). For clarity, approximately 5% of the data points were removed from this graph as outliers, determined using the standard interquartile range method from statistical analysis.

Table 4 summarizes the median demands (that is, required capacities) to meet the minimum ACMR limits in Table 3 for each archetype. These demands are discussed in more detail in the following sections.

Maximum interstory drift

Maximum interstory drift demand Δ_{story} was calculated using the lateral displacements of the two columns in each story of each archetype frame. For each column, the story drift was calculated by dividing the relative horizontal displacement of the work points immediately above and below the story by the height of the story. The larger of the two drift values from these columns was taken as the governing interstory drift and the largest drift across all stories was taken as the maximum interstory drift for the archetype.

The analysis results in Table 4 show an overall median Δ_{story} demand of 4.21%, with a coefficient of variation of 1.46 (with outliers removed [about 5% of the data], the median demand was 4.13%, with a coefficient of variation of 0.33). Across the performance groups, the median Δ_{story} demand ranged from 4.11% to 4.35%. However, the design of the braces is typically based on brace axial deformations estimated using an idealized shear frame assumption.[8] This is investigated in the section titled "Maximum Design Story Drift."

Maximum design story drift

As described in Oh et al.[8] and Kersting et al.,[23] the brace axial deformations Δ_b used in the design of a buckling-restrained frame structure are typically determined based on an idealized shear frame assumption that ignores the axial deformations of the beam and column components of the frame. This approximation uses Eq. (3) to estimate Δ_b, which is then used to design the braces.

$$\Delta_b = \sqrt{h^2 + \left(w + \Delta_{d,max} h\right)^2} - L_T \tag{3}$$

where

h = work point–to–work point height of the brace, where the work points are located at the intersections of the brace centerline with the centerlines of the beam and column components of the frame

w = work point–to–work point horizontal projection length of the brace

The maximum brace axial deformation demand $\Delta_{b,max}$ from each dynamic analysis of each archetype was used as Δ_b in Eq. (3) to back calculate the corresponding maximum design story drift demand $\Delta_{d,max}$. The median $\Delta_{d,max}$ demand across all archetypes was 3.87% (Table 4), with a coefficient of variation of 1.73 (3.76% and 0.34, respectively, with outliers removed). The range of median $\Delta_{d,max}$ across the performance groups was 3.77% to 4.00%, indicating that brace deformations calculated from a maximum design story drift $\Delta_{d,max}$ of 4% should be targeted in future design and experimental testing to demonstrate ductile behavior of the novel brace. The archetypes in this paper were designed for a smaller maximum design story drift $\Delta_{d,max}$ of 3%. The possible implications of this discrepancy in the design of the archetypes are considered in the subsequent sections.

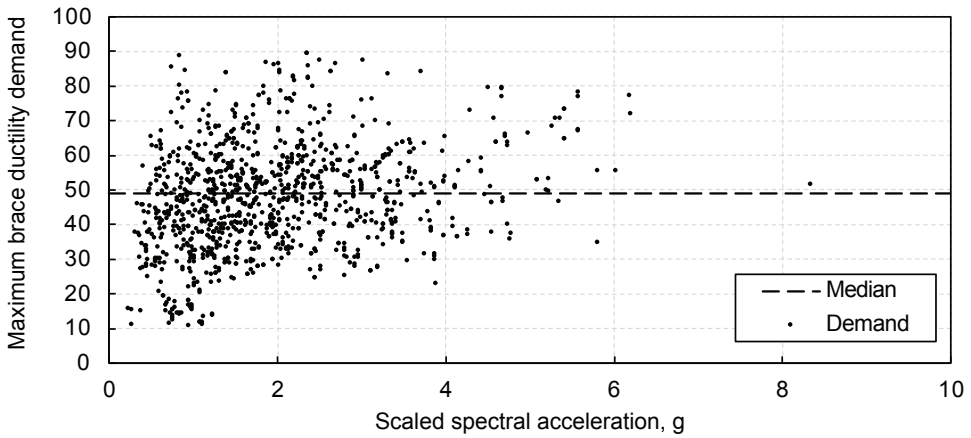

Figure 6. Maximum brace ductility demands, with outliers removed.

Table 4. Maximum demands under ground motion set scaled to median collapse intensity for each archetype

Performance group	Archetype design identifier*	Median demands					
		μ_{max}	μ_c	$\Delta_{b,gap}$, in.	$\Delta_{d,max}$, %	Δ_{story}, %	$\Delta_{d,max}/\Delta_{story}$
1	1SD1	51	291	2.74	3.75	4.03	0.93
	1SD2	49	282	2.89	4.09	4.47	0.92
	1SD3	49	303	2.72	3.81	4.24	0.90
	Group 1 median	50	291	2.80	3.86	4.25	0.92
2	2SD1	51	260	2.71	3.68	4.03	0.92
	2SD2	49	290	2.74	3.80	4.14	0.92
	2SD3	52	311	2.77	3.89	4.27	0.91
	4SD1	51	285	4.46	3.64	3.92	0.93
	4SD2	48	261	4.45	3.65	3.98	0.92
	Group 2 median	50	279	3.24	3.77	4.13	0.92
3	1SD6	49	308	2.73	4.02	4.34	0.93
	1SD9	46	292	2.29	3.36	3.72	0.92
	2SD6	46	278	2.75	3.90	4.33	0.91
	2SD9	46	323	2.58	3.74	4.03	0.92
	Group 3 median	46	297	2.63	3.78	4.11	0.92
4	2CC1	51	262	2.71	3.69	3.96	0.94
	2CC2	49	274	2.97	4.04	4.43	0.95
	2CC3	51	256	2.86	3.88	4.16	0.93
	5CC1	50	259	2.31	3.97	4.13	0.96
	5CC2	51	290	2.52	4.28	4.60	0.93
	Group 4 median	51	271	2.65	3.94	4.25	0.94
5	2CC4	48	245	2.98	4.07	4.33	0.93
	2CC6	47	267	2.87	3.90	4.30	0.93
	2CC9	50	256	2.95	4.01	4.39	0.93
	Group 5 median	48	258	2.94	4.00	4.33	0.93
6	2ZZ2	49	290	2.74	3.80	4.14	0.92
	2ZZ3	53	312	2.76	3.90	4.26	0.91
	4ZZ2	48	261	4.45	3.65	3.98	0.92
	Group 6 median	49	285	3.09	3.77	4.15	0.91
7	2ZZ4	49	275	2.78	3.80	4.22	0.90
	2ZZ6	47	270	2.89	4.13	4.51	0.91
	2ZZ9	47	308	2.65	3.85	4.24	0.90
	Group 7 median	48	283	2.78	3.95	4.35	0.91
Overall median		49	280	2.84	3.87	4.21	0.92

Note: $\Delta_{b,gap}$ = maximum brace end gap closure; $\Delta_{d,max}$ = maximum design story drift; Δ_{story} = maximum interstory drift, μ_c = maximum cumulative brace ductility; μ_{max} = maximum brace ductility.

* The first character is the building plan number, the next two characters indicate the brace configuration (SD for single diagonal, ZZ for zigzag, and CC for chevron), and the last character is the number of stories.

To evaluate the accuracy of the simplified shear frame assumption used in design, Table 4 also provides the median ratio of the maximum design story drift demand $\Delta_{d,max}$ (calculated from the maximum brace axial deformation demand $\Delta_{b,max}$) to the corresponding maximum interstory drift demand Δ_{story} (the actual interstory drift demand calculated from the top and bottom work-point lateral displacements of all columns in the structure) from the dynamic analyses of each archetype. The results show a median ratio of 0.92 across all archetypes, with a coefficient of variation of 0.02. Thus, the maximum design story drift demand $\Delta_{d,max}$ was consistently slightly smaller than the actual maximum interstory drift Δ_{story}, which can be attributed to the fact that braced frames do not exhibit perfect shear story behavior. Specifically, elongations of the column and beam components after cracking allow the structure to reach greater interstory drifts than a perfect shear frame with the same brace deformations. These results confirm that the shear frame assumption used in design is slightly conservative and reasonable, allowing for a simple design procedure for the braces.

Maximum brace ductility

The maximum brace ductility demand μ_{max} was calculated as follows:

$$\mu_{max} = \Delta_{b,max}/\Delta_{by}$$

where

Δ_{by} = brace axial deformation at yield of the energy-dissipation bars

The maximum brace ductility demand was calculated as the absolute sum (that is, total range) of the maximum compression and tension brace ductility demands over the entire dynamic analysis history. For example, if a brace experienced a maximum tension ductility demand of +35 and a maximum compression ductility demand of –10 during an earthquake, the corresponding maximum brace ductility demand μ_{max} was calculated as (35) – (-10) = 45.

The analysis results in Table 4 show an overall median μ_{max} demand of 49 with a coefficient of variation of 1.32 (48 and 0.31, respectively, with outliers removed). To satisfy FEMA P695 requirements, the brace ductility capacity should be at least equal to the largest median demand out of all performance groups. Thus, based on the performance group median demands in Table 4, future experimental research should demonstrate a brace ductility μ_{max} of 51 to satisfy the target seismic performance factors under the FEMA P695 procedure. Because the ductility capacity of the proposed brace is governed by the performance of the energy-dissipation bars, a total strain range of approximately 0.11 would achieve this target performance for braces using Grade 60 (410 MPa) energy-dissipation bars. The test results in Rodriguez et al.[22] show that this total strain range is achievable for reinforcing bars that are prevented from buckling.

To provide additional insight into the brace strain demands, **Figure 7** shows the maximum tension and compression strains within the 0.11 strain range limit for 148 of the most critical maximum brace ductility demands from the dynamic analyses of the archetypes. The results show a maximum compression strain demand of about 0.08 and a maximum tension strain demand of about 0.09, which exceeds the maximum usable tensile strain limit $\varepsilon_{s,max}$ of 0.06 that was assumed in the design of the archetype frames. This discrepancy occurred because the unbonded lengths of the energy-dissipation bars in the arche-

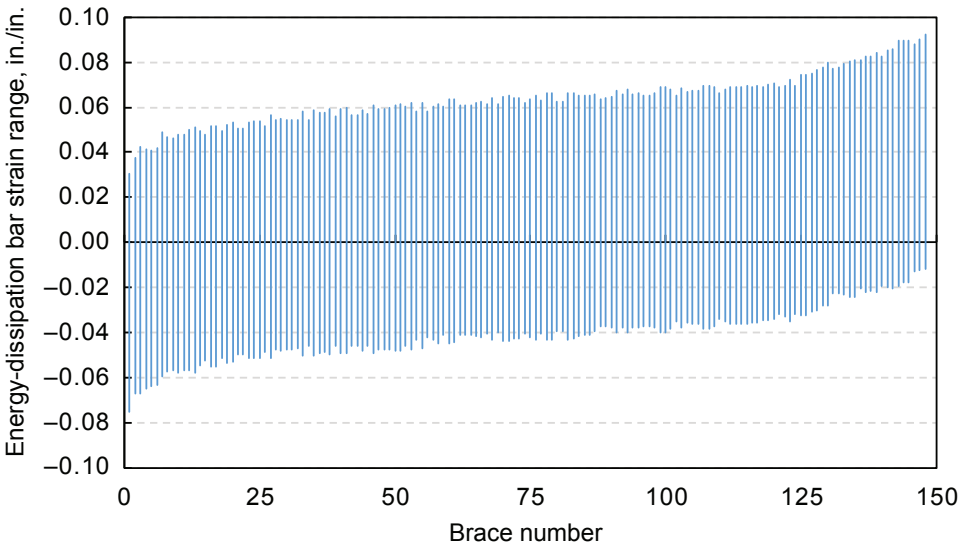

Figure 7. Maximum tension and compression strain demands for 148 most critical braces.

types were designed for a maximum design story drift $\Delta_{d,max}$ of 3%, which is smaller than the maximum demand of 4% from the dynamic analyses of the archetypes. The energy-dissipation bar strains would be within the ±0.06 range for future archetypes with longer unbonded lengths designed based on the recommended maximum design story drift of 4%. As such, future experimental testing of braces should consider symmetric cyclic loading to approximately ±0.06 strain in the energy-dissipation bars, which would also satisfy the total strain range of 0.11 obtained from the dynamic analyses.

If future experimental studies discover that the ±0.06 strain range is not achievable for the energy-dissipation bars, further increasing the unbonded lengths of the braces may be effective in lowering the maximum strain demands. Increasing the unbonded length spreads the brace deformations over a longer length of the bars, reducing the maximum bar strains reached at the same story drift. However, this change would also reduce the bonded lengths of the braces, which may negatively affect the intended performance of the brace in these regions in providing development length for the energy-dissipation bars and additional stiffness to the brace in compression.

Maximum cumulative brace ductility

The maximum cumulative brace ductility demand μ_c was calculated as follows:

$$\mu_c = \Sigma\Delta_{b,inelastic}/\Delta_{by}$$

where

$\Delta_{b,inelastic}$ = inelastic brace axial deformation (the Σ in the equation indicates the summation of the inelastic brace deformations over the entire dynamic response history)

As shown in Table 4, the overall median maximum cumulative brace ductility demand μ_c from the dynamic analyses of the archetypes was 280 with a coefficient of variation of 0.65 (274 and 0.39, respectively, with outliers removed). The median demands for the different performance groups ranged from 258 to 297. Thus, a target cumulative brace ductility μ_c of 297 is recommended to result in archetypes that satisfy FEMA P695 performance criteria, which corresponds to a total cumulative inelastic strain of approximately 0.62 for Grade 60 (410 MPa) energy-dissipation bars. Based on the test results in Rodriguez et al.,[22] this cumulative inelastic strain capacity is achievable for reinforcing bars that are prevented from buckling. If deemed necessary based on future experiments, it may be possible to reduce the maximum cumulative strain demands of the energy-dissipation bars by increasing the length of the unbonded regions, similar to the maximum strain demands discussed in the previous section.

Maximum brace end gap closure

The proposed reinforced-concrete brace can fail if both end gaps fully close, causing the brace concrete to bear directly against the corbel region. Ensuring that the gap width is large enough to prevent this failure mode while also small enough to minimize the laterally unsupported length of the energy-dissipation bars is critical to the design of the braces. Thus, the maximum end gap closure demand $\Delta_{b,gap}$ has important implications for achieving the aforementioned brace ductility capacities by quantifying the minimum required width of the end gaps.

The maximum brace end gap closure demands were determined from the maximum axial deformation demands of the braces in compression. Table 4 shows a median gap closure demand $\Delta_{b,gap}$ of 2.84 in. (72.1 mm) for each end gap with a coefficient of variation of 1.00 (2.75 in. [70.0 mm] and 0.35, respectively, with outliers removed). The median $\Delta_{b,gap}$ demands across the performance groups ranged from 2.63 to 3.24 in. (66.8 to 82.3 mm); however, archetypes 4SD1, 4SD2, and 4ZZ2 had significantly larger gap closure demands of 4.46, 4.45, and 4.45 in. (113, 113, and 113 mm), respectively. This may be expected because these archetypes had larger story heights of 25 ft (7.6 m), resulting in larger brace deformations and, thus, larger gap closures based on the design procedure described in Oh et al.[9] Looking only at the archetypes with a 15 ft (4.6 m) story height, the overall median maximum brace end gap closure $\Delta_{b,gap}$ was 2.74 in. (69.6 mm) with a coefficient of variation of 0.60 (2.68 in. [68.1 mm] and 0.33, respectively, with outliers removed), and the performance group medians ranged from 2.63 to 2.94 in. (66.8 to 74.7 mm).

From these results, a minimum end gap width of approximately 3 in. (76 mm) was needed for the archetypes with 15 ft (4.6 m) story height in this study, while a gap width of about 5 in. (127 mm) should be designed for structures with 25 ft (7.6 m) story height. Both of these values are consistent with the design gap widths calculated using a maximum design story drift $\Delta_{d,max}$ of 4% under the design procedures of Oh et al.[9] This provides further evidence that, in order to result in archetypes that satisfy FEMA P695 performance criteria, the brace deformation demands should be determined based on a target design story drift of 4%.

Conclusion

This study investigated the minimum capacities needed for the proposed reinforced-concrete buckling-restrained brace in precast concrete braced frames that satisfy FEMA P695 performance criteria for seismic design category D_{max} and a response modification coefficient (R factor) of 8. A set of 26 archetype braced frames were designed to represent the expected design space of the structural system. Nonlinear static pushover analyses were conducted to determine the system overstrength factor and to ensure that the archetypes were not overdesigned. Then, incremental nonlinear dynamic response history analyses were conducted to quantify the maximum demands under a set of 44 ground motion records collectively scaled to the median collapse intensity for each archetype per FEMA P695. The following conclusions from this paper may

be limited to the archetype frames designed for the study, the numerical modeling and analysis parameters, and the minimum ACMR limits used in the demand quantification:

- Precast concrete frames using the proposed brace have lower lateral stiffness compared with precast concrete frames using conventional steel buckling-restrained braces. This difference is largely due to the cracking of concrete and the higher grade of steel (Grade 60 [410 MPa]) for the energy-dissipation bars in concrete braces compared with lower steel yield strengths in steel braces.

- The simplified shear frame assumption provides a conservative and reasonable approximation to determine the brace axial deformations at the maximum design story drift $\Delta_{d,max}$.

- For structures in high seismic regions, the unbonded lengths and end gap widths of the braces should be designed for a maximum design story drift $\Delta_{d,max}$ of 4% using the aforementioned shear frame assumption. Based on the maximum brace end gap closure demands $\Delta_{b,gap}$ for the archetypes in this study, the required end gap width was 3 in. (76 mm) for frames with 15 ft (4.6 m) story heights and 4.5 in. (114 mm) for frames with 25 ft (7.6 m) story heights.

- Braces with capacities meeting at least a ductility μ_{max} of 51 and a cumulative ductility μ_c of 297 are needed for braced frame structures in high seismic regions to satisfy the median collapse performance criteria in FEMA P695.

- For archetypes designed using the recommended maximum design story drift of 4%, experimental testing of braces should consider symmetric cyclic loading to ±0.06 strain range in the energy-dissipation bars in order to reach the aforementioned brace ductility capacities.

The study described in this paper is not a FEMA P695 study to validate seismic performance factors (for example, *R* factor) by modeling the failure and collapse of the new braced frame system. Rather, the paper uses the FEMA P695 methodology and prescribed earthquake ground motions to guide future experimental research on minimum capacities that brace specimens intended for high seismic application should be designed and validated for through testing. In accordance with this aim, the braces in the archetype structures analyzed in the paper were assumed to be designed such that their failure occurs beyond these minimum capacities. As such, modeling the failure of the braces was not targeted in the numerical analyses.

Future experimental research is needed to demonstrate that the new brace can be designed and detailed to achieve the recommended target performance limits (minimum capacities). After such successful future testing, the ultimate adoption of this braced frame system will require a FEMA P695 study using numerical models that can accurately capture failure based on the experimental results. These tests should include isolated braces, braced frame subassemblies, and multistory frames and buildings including different brace configurations (such as chevron and single diagonal) to provide substantial experimental validation for this novel system.

Acknowledgments

This research was conducted with the sponsorship of PCI under a Daniel P. Jenny Research Fellowship. The authors acknowledge the support of the PCI Research and Development Council, PCI Central Region, and the members of the industry advisory committee, including Anshul Agarwal of Consulting Engineers Group, Suzanne Aultman of Metromont Corp., Keith Bauer of Buehler Engineering, Jared Brewe of PCI, Harry Gleich of Gleich Engineering and Associates LLC, Kevin Kirkley of Tindall Corp., Mitchel Le Heux of Englekirk Structural Engineers, Laura Redmond of Clemson University, Jose Restrepo of the University of California San Diego, Brandon Ross of Clemson University, and Kim Seeber of Seaboard Services. In addition, this research was supported by a University of Notre Dame Deans' Fellowship granted to Shane Oh, as well as an American Concrete Institute Foundation Barbara S. and W. Calvin McCall Carolinas Fellowship and an American Society of Civil Engineers O. H. Ammann Research Fellowship in Structural Engineering granted to Lily Pearson. Any opinions, findings, conclusions, and recommendations expressed in the paper are those of the authors and do not necessarily reflect the views of the individuals and organizations acknowledged herein.

References

1. Clark, P., I. D. Aiken, E. Ko, K. Kasai, and I. Kimura. 1999. "Design Procedures for Buildings Incorporating Hysteretic Damping Devices." In *Proceedings of the 68th Annual Convention of the Structural Engineers Association of California*, 355–371. Sacramento, CA: Structural Engineers Association of California.

2. Clark, P., K. Kasai, I. D. Aiken, and I. Kimura. 2000. "Evaluation of Design Methodologies for Structures Incorporating Steel Unbonded Braces for Energy Dissipation." In *Proceedings of the 12th World Conference on Earthquake Engineering*. Upper Hutt, New Zealand: New Zealand Society for Earthquake Engineering. https://www.iitk.ac.in/nicee/wcee/article/2240.pdf.

3. Sabelli, R., S. Mahin, and C. Chang. 2003. "Seismic Demands on Steel Braced-Frame Buildings with Buckling-Restrained Braces." *Engineering Structures* 25 (5): 655–666. https://doi.org/10.1016/S0141-0296(02)00175-X.

4. Wang, Y., L. Ibarra, and C. Pantelides. 2016. "Seismic Retrofit of a Three-Span RC Bridge with Buckling-Restrained Braces." *Journal of Bridge Engineering* 21 (11):

04016073. https://doi.org/10.1061/(ASCE)BE.1943-5592.0000937.

5. Viano, J. D., and T. C. Schaeffer. 2017. "Novel Use of Buckling-Restrained Braces in Precast Concrete Frames." *PCI Journal* 62 (5): 28–34. https://doi.org/10.15554/pcij62.5-03.

6. Guerrero, H, T. Ji, J. A. Escobar, and A. Teran-Gilmore. 2018. "Effects of Buckling-Restrained Braces on Reinforced Concrete Precast Models Subjected to Shaking Table Excitation." *Engineering Structures* 163: 294–310. https://doi.org/10.1016/j.engstruct.2018.02.055.

7. El-Bahey, S., and M. Bruneau. 2011. "Buckling Restrained Braces as Structural Fuses for the Seismic Retrofit of Reinforced Concrete Bridge Bents." *Engineering Structures* 33 (3): 1052–1061. https://doi.org/10.1016/j.engstruct.2010.12.027.

8. Oh, S., Y. C. Kurama, J. Mohle, and B. W. Saxey. 2021. "Seismic Design and Analysis of Precast Concrete Buckling-Restrained Braced Frames." *PCI Journal* 66 (5): 54–83.

9. Oh, S., Y. C. Kurama, J. Mohle, L. Polster, M. Manning, and B. Weldon. 2023. "A Novel Reinforced-Concrete Buckling-Restrained Brace for Precast Concrete Lateral Load-Resisting Frames." *PCI Journal* 68 (3): 95–116.

10. Oh, S., L. Polster, M. Manning, J. Mohle, B. Weldon., and Y. C. Kurama, 2023. "Experimental Investigation of a Novel Reinforced Concrete Buckling-Restrained Brace." *PCI Journal* 68 (6): 65–91.

11. FEMA (Federal Emergency Management Agency). 2009. *Quantification of Building Seismic Performance Factors*. FEMA P695. Washington, DC: FEMA.

12. ASCE (American Society of Civil Engineers) and SEI (Structural Engineering Institute). 2022. *Minimum Design Loads and Associated Criteria for Buildings and Other Structures*. ASCE/SEI 7-22. Reston, VA: ASCE. https://doi.org/10.1061/9780784415788.

13. Kessler, H. D., K. M. Conway, L. M. Redmond, and G. J. Pataky. 2023. "Design and Cyclic Testing of a Gusset Plate Connection for Precast Concrete Buckling-Restrained Braced Frames." *PCI Journal* 68 (2): 30–51. https://doi.org/10.15554/pcij68.2-03.

14. ASTM Subcommittee A01.05. 2016. *Standard Specification for Deformed and Plain Low-Alloy Steel Bars for Concrete Reinforcement*. ASTM A706/A706M. West Conshohocken, PA: ASTM International.

15. ASCE and SEI. 2016. *Minimum Design Loads and Associated Criteria for Buildings and Other Structures*. ASCE/SEI 7-16. Reston, VA: ASCE. https://doi.org/10.1061/9780784415788.

16. Kurama, Y., S. Sritharan, R. Fleischman, J. Restrepo, R. Henry, N. Cleland, S. K. Ghosh, and P. Bonelli. 2018. "Seismic-Resistant Precast Concrete Structures: State of the Art," *Journal of Structural Engineering* 144 (4): 03118001.

17. ACI (American Concrete Institute) Committee 318. 2019. *Building Code Requirements for Structural Concrete (ACI 318-19) and Commentary (ACI 318R-19).* Farmington Hills, MI: ACI.

18. Aragon, T. A., Y. C. Kurama, and D. F. Meinheit. 2020. "Behavior of Ductile Short-Grouted Seismic Reinforcing Bar-to-Foundation Connections under Adverse Construction Conditions." *PCI Journal* 65 (4): 33–50. https://doi.org/10.15554/pcij65.4-01.

19. Cervenka, V., J. Cervenka, and R. Pukl. 2002. "ATENA—A Tool for Engineering Analysis of Fracture in Concrete." *Sadhana* 27 (4): 485–492. https://doi.org/10.1007/BF02706996.

20. ACI Innovation Task Group 5. 2019. *Requirements for Design of a Special Unbonded Post-Tensioned Precast Shear Wall Satisfying ACI 550.6 (ACI 550.7) and Commentary*. Farmington Hills, MI: ACI.

21. Smith, B. J., and Y. C. Kurama. 2014. "Seismic Design Guidelines for Solid and Perforated Hybrid Precast Concrete Shear Walls." *PCI Journal* 59 (3): 43–59. https://doi.org/10.15554/pcij.06012014.43.59.

22. Rodriguez, M. E., J. C. Botero, and J. Villa. 1999. "Cyclic Stress-Strain Behavior of Reinforcing Steel Including Effect of Buckling." *Journal of Structural Engineering* 125 (6): https://doi.org/10.1061/(ASCE)0733-9445(1999)125:6(605).

23. Kersting, R. A., L. A. Fahnestock, and W. A. López. 2015. *Seismic Design of Steel Buckling-Restrained Braced Frames: A Guide for Practicing Engineers*. NEHRP (National Earthquake Hazards Reduction Program) Seismic Design Technical Brief 11. Gaithersburg, MD: National Institute of Standards and Technology. https://doi.org/10.6028/NIST.GCR.15-917-34.

Notation

A_b = effective area of bonded regions

A_{ED} = total area of energy-dissipation bars

A_s = total area of longitudinal reinforcing bars

A_{sT} = total area of terminated longitudinal reinforcing bars

A_{ut} = uncracked transformed area of reinforced concrete section

C_d = deflection amplification factor per ASCE/SEI 7-16

d_b = diameter of energy-dissipation bar

D_{max} = upper bound of seismic design category D per FEMA P695

E_b = effective modulus of elasticity of bonded regions

E_c = modulus of elasticity of concrete

E_s = modulus of elasticity of energy-dissipation bars

f'_c = specified design compressive strength of concrete

f_{sy} = specified design yield strength of reinforcing bars

$f_{y,max}$ = maximum expected yield strength of energy-dissipation bars

$f_{y,min}$ = minimum expected yield strength of energy-dissipation bars

h = work point–to–work point height of brace

k_b = effective axial stiffness of bonded regions

k_{ub} = effective axial stiffness of unbonded regions

KF = stiffness modification factor

L_b = length of bonded regions

L_T = total work point–to–work point diagonal length of brace

L_{ub} = total length of unbonded regions at both ends of brace

$L_{ub,add}$ = total additional unbonded length due to debonding of the energy-dissipation bars

M_u = factored design moment of beam or column

N_u = factored design axial force of brace

P_u = factored design axial force of beam or column

R = seismic response modification coefficient per ASCE/SEI 7-16

S_{ct} = median collapse intensity

w = work point–to–work point horizontal projection length of brace

α_b = coefficient quantifying effective additional unbonded length due to debonding of the energy-dissipation bars

Δ_b = brace design axial deformation

$\Delta_{b,gap}$ = maximum brace end gap closure

$\Delta_{b,inelastic}$ = inelastic brace axial deformation

$\Delta_{b,max}$ = maximum brace axial deformation

Δ_{by} = brace axial deformation at yield of energy-dissipation bars

$\Delta_{d,max}$ = maximum design story drift

Δ_{story} = maximum interstory drift

$\varepsilon_{s,max}$ = design usable tensile strain limit of energy-dissipation bars

μ_c = maximum cumulative brace ductility

μ_{max} = maximum brace ductility

ω = strain hardening factor

Ω_0 = system overstrength factor per ASCE/SEI 7-16

About the authors

Shane Oh, PhD, graduated from the Department of Civil and Environmental Engineering and Earth Sciences at the University of Notre Dame in Notre Dame, Ind.

Jon Mohle, SE, is a senior product and market manager at Clark Pacific in Sacramento, Calif.

Lily A. Pearson, MSc, is a project engineer at Frost Engineering & Consulting in Mishawaka, Ind.

Mark P. Manning, PhD, was a research scientist in the Department of Civil and Environmental Engineering and Earth Sciences at the University of Notre Dame.

Brad D. Weldon, PhD, is a teaching professor in the Department of Civil and Environmental Engineering and Earth Sciences at the University of Notre Dame.

Yahya C. Kurama, PhD, PE, is a professor in the Department of Civil and Environmental Engineering and Earth Sciences at the University of Notre Dame.

Abstract

This study numerically investigated the dynamic seismic response of multistory precast concrete frame structures using a novel reinforced-concrete buckling-restrained brace component. The maximum demands on the braces were quantified with the intent to guide future experimental testing and validation according to the collapse performance requirements of FEMA P695. A set of 26 braced frame archetypes were designed using seismic procedures consistent with current U.S. building code requirements, and effective linear-elastic as well as nonlinear numerical models of these frame structures were developed. In addition to monotonic static pushover analyses, the nonlinear archetype models were subjected to a set of 44 scaled ground motion records to quantify the system overstrength factor, maximum interstory drift, design story drift, brace ductility, cumulative brace ductility, and end gap closure. It was found that braces designed for a maximum design story drift of 4% and demonstrating ductility capacities of at least 51 and cumulative ductility capacities of at least 297 are needed for braced frame structures in high seismic regions to satisfy the median collapse performance criteria in FEMA P695.

Keywords

Ductility, gap closure, FEMA P695, incremental dynamic response history analysis, monotonic static pushover analysis, precast concrete buckling-restrained braced frame lateral system, reinforced-concrete buckling-restrained brace, response modification coefficient, seismic design demands, seismic performance factor, story drift, system overstrength factor

Review policy

This paper was reviewed in accordance with the Precast/Prestressed Concrete Institute's peer-review process. The Precast/Prestressed Concrete Institute is not responsible for statements made by authors of papers in PCI Journal. No payment is offered.

Publishing details

This paper appears in *PCI Journal* (ISSN 0887-9672) V. 69, No. 6, November-December 2024, and can be found at https://doi.org/10.15554/pcij69.6-02. *PCI Journal* is published bimonthly by the Precast/Prestressed Concrete Institute, 8770 W. Bryn Mawr Ave., Suite 1150, Chicago, IL 60631.

Reader comments

Please address any reader comments to *PCI Journal* editor-in-chief Tom Klemens at tklemens@pci.org or Precast/Prestressed Concrete Institute, c/o *PCI Journal*, 8770 W. Bryn Mawr Ave., Suite 1150, Chicago, IL 60631.